ASSESSMENT OF FRAGMENTATION PERFORMANCE OF BLAST-ENHANCED EXPLOSIVE FRAGMENTATION MUNITIONS

V. M. Gold, Y. Wu, and W. J. Poulos

[1]*US Army RDECOM-ARDEC, Attn: AMSRD-AAR-MEE-W, Bldg. 3022, Picatinny Arsenal, New Jersey, 07806-5000, USA*

ABSTRACT

A new modeling and experimentation methodology for assessing fragmentation characteristics of blast-enhanced explosive fragmentation munitions had been developed. Fragmentation performance of two high explosive compositions had been examined in this work: a baseline, PBXN-9 (92% HMX, 6% Dioctyl adipate, 2% Hycar 4454) explosive, and an aluminized blast-enhanced PAX-Al composition. The experimental assessment of the fragmentation performance of tested charges was accomplished using the fragmentation arena tests, the sawdust fragment recovery experimentation, and the flash-screen fragment velocity tests. The analytical assessment of the thermodynamic parameters of the PBXN-9 and the PAX-Al compositions was performed employing the JAGUAR code. The analytical assessment of the fragmentation parameters of the explosive fragmentation charges was performed employing the PAFRAG (Picatinny Arsenal Fragmentation) modeling methodology linking the three-dimensional axial symmetric high-strain high-strain-rate hydrocode analyses with a phenomenological fragmentation model based on the Mott's theory of break-up of ideal cylindrical "ring-bombs". For the PBXN-9 explosive, the PAFRAG modeling has been shown to accurately reproduce the available experimental data, both the fragmentation and the fragment velocity measurements. However, for the PAX-Al explosive, a significant discrepancy between the fragment recovery data and the flash-screen velocity data had been noted and examined. In particular, based on the fragment recovery data, the coupled PAFRAG/thermodynamic analyses indicated that the amount of the aluminum contributing to the momentum of the fragments had to be in the order of approximately 20% of the total available, 80% of the aluminum remaining unreacted. Conversely, from the flash-panel velocity data, the entire 100% aluminum available had to react to agree with the relatively fast fragment time of arrivals measured. The data confidence level of the flash-panel velocity technique had been examined, indicating approximately 30% data uncertainty margins possible. Accordingly, the entire 100% aluminum reaction may or may not be feasible, but a fair chance of approximately 20% of the aluminum contributing to the fragment kinetic energies had been concluded.

FRAGMENTATION MODELING AND EXPERIMENTATION

Modeling performance of the enhanced-blast explosive fragmentation munitions presented in this work was performed employing the PAFRAG (Picatinny Arsenal Fragmentation) modeling methodology[1] which links three-dimensional axial symmetric high-strain high-strain-rate CALE[2] hydrocode analyses with a semi-empirical fragmentation model PAFRAG-Mott[3]. CALE is a plane two-dimensional and three-dimensional axial symmetric high rate finite difference computer program based on Arbitrary Lagrangian-Eulerian formulation of the governing equations.

The geometry of an example problem considered in this work is shown in Fig. 1. Upon initiation of the high explosive charges, rapid expansion of high pressure detonation products results in high-strain high-strain-rate dilation of the hardened steel shell, which eventually ruptures generating a "spray" of high-velocity steel fragments. Defining the longitudinal axis of the munition as the polar axis *z*, the resulting flight trajectories of the fragment spray can be referenced using the polar altitudinal angles Θ measured from the munition's nose (Θ=0°) to tail (Θ=180°).

Report Documentation Page

Form Approved
OMB No. 0704-0188

1. REPORT DATE	2. REPORT TYPE	3. DATES COVERED
OCT 2010	**N/A**	**-**

4. TITLE AND SUBTITLE	5a. CONTRACT NUMBER
Assessment Of Fragmentation Performance Of Blastenhanced Explosive Fragmentation Munitions	5b. GRANT NUMBER
	5c. PROGRAM ELEMENT NUMBER
6. AUTHOR(S)	5d. PROJECT NUMBER
	5e. TASK NUMBER
	5f. WORK UNIT NUMBER
7. PERFORMING ORGANIZATION NAME(S) AND ADDRESS(ES) **US Army RDECOM-ARDEC, Attn: AMSRD-AAR-MEE-W, Bldg. 3022, Picatinny Arsenal, New Jersey, 07806-5000, USA**	8. PERFORMING ORGANIZATION REPORT NUMBER
9. SPONSORING/MONITORING AGENCY NAME(S) AND ADDRESS(ES)	10. SPONSOR/MONITOR'S ACRONYM(S)
	11. SPONSOR/MONITOR'S REPORT NUMBER(S)

12. DISTRIBUTION/AVAILABILITY STATEMENT

Approved for public release, distribution unlimited

13. SUPPLEMENTARY NOTES

See also ADA550809. Military Aspects of Blast and Shock (MABS 21) Conference proceedings held on October 3-8, 2010. Approved for public release; U.S. Government or Federal Purpose Rights License., The original document contains color images.

14. ABSTRACT

A new modeling and experimentation methodology for assessing fragmentation characteristics of blast-enhanced explosive fragmentation munitions had been developed. Fragmentation performance of two high explosive compositions had been examined in this work: a baseline, PBXN-9 (92% HMX, 6% Dioctyl adipate, 2% Hycar 4454) explosive, and an aluminized blast-enhanced PAX-Al composition. The experimental assessment of the fragmentation performance of tested charges was accomplished using the fragmentation arena tests, the sawdust fragment recovery experimentation, and the flash-screen fragment velocity tests. The analytical assessment of the thermodynamic parameters of the PBXN-9 and the PAX-Al compositions was performed employing the JAGUAR code. The analytical assessment of the fragmentation parameters of the explosive fragmentation charges was performed employing the PAFRAG (Picatinny Arsenal Fragmentation) modeling methodology linking the three-dimensional axial symmetric high-strain high-strain-rate hydrocode analyses with a phenomenological fragmentation model based on the Motts theory of break-up of ideal cylindrical ringbombs. For the PBXN-9 explosive, the PAFRAG modeling has been shown to accurately reproduce the available experimental data, both the fragmentation and the fragment velocity measurements. However, for the PAX-Al explosive, a significant discrepancy between the fragment recovery data and the flash-screen velocity data had been noted and examined. In particular, based on the fragment recovery data, the coupled PAFRAG/thermodynamic analyses indicated that the amount of the aluminum contributing to the momentum of the fragments had to be in the order of approximately 20% of the total available, 80% of the aluminum remaining unreacted. Conversely, from the flash-panel velocity data, the entire 100% aluminum available had to react to agree with the relatively fast fragment time of arrivals measured. The data confidence level of the flash-panel velocity technique had been examined, indicating approximately 30% data uncertainty margins possible. Accordingly, the entire 100% aluminum reaction may or may not be feasible, but a fair chance of approximately 20% of the aluminum contributing to the fragment kinetic energies had been concluded.

15. SUBJECT TERMS

16. SECURITY CLASSIFICATION OF:			17. LIMITATION OF ABSTRACT	18. NUMBER OF PAGES	19a. NAME OF RESPONSIBLE PERSON
a. REPORT	b. ABSTRACT	c. THIS PAGE			
unclassified	**unclassified**	**unclassified**	**SAR**	**16**	

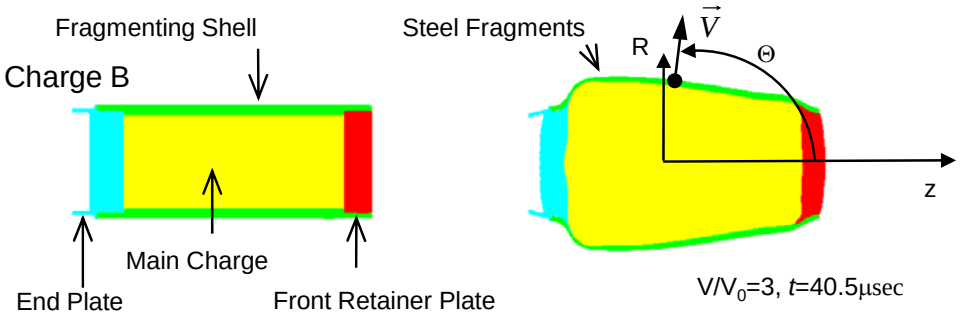

Fig. 1 Results of CALE-code modeling: initial configuration and CALE's predictions following the explosive detonation initiation.

In fragmentation arena tests, the ammunition fragmentation characteristics are assessed as functions of polar angles Θ identifying angular positions of fragment-catching witness panels and velocity-measuring screens. In PAFRAG code analyses, positions of these devices are irrelevant, and the fragmentation characteristics are assessed in reference to the fragment trajectory angles Θ' calculated from the CALE code cell velocities at the time of the shell break-up. Once the shell breaks up and fragments are formed, fragment velocities may change with time due to a number of reasons, including the air drag and the rigid body lateral and tumbling motion induced at the time of the case fracture. The rate at which fragments can dissipate the available kinetic energy is a strong function of the fragment mass and shape, therefore, the velocity-measuring-screen devices are prone to large errors and data uncertainties, mostly because of an innate statistical variance in the fragment spray mass and the shape. The PAFRAG mathematical model for the air drag will be addressed in more details in the later section. Assuming that the fragment trajectory angles Θ' do not change with time (that is the lateral drift of fragments due to the initial rigid body motion, the air resistance and tumbling is relatively small) and that the definitions of angles Θ and Θ' are approximately identical, the PAFRAG model enables prediction of crucial characteristics of explosive fragmenting munitions including the number of fragments, the fragment size distribution, and the average fragment velocities.

The mathematical description of the PAFRAG-Mott model is given here for completeness. The PAFRAG-Mott fragment distribution is defined as

$$N(m) = \sum_{j}^{L} N_{0j} e^{-\left(m/\mu_j\right)^{1/2}} \tag{1}$$

In equation (1) $N(m)$ represents total number of fragments of mass greater than m. For computational purposes, in PAFRAG code, the shell is "divided" into a finite number of short "ring" segments, L, each "ring" j corresponding to the respective fragment spray Θ-angle trajectory, Θ_j. For each ring element j uniform field variables are assumed, and the values of the total fragment mass, m_j, the average fragment velocity, V_j, and the shell break-up radius, r_j, are calculated. In equation (1), μ_j and N_{0j} denote the one half of the average fragment mass and the total number of fragments projected from the "ring" j at the trajectory angles Θj, respectively. The values of μ_j and N_{0j} are determined through the following relationships:

$$\mu_j = \sqrt{\frac{2}{\rho}}\left(\frac{\sigma_F}{\gamma}\right)^{3/2}\left(\frac{r_j}{V_j}\right)^3 \tag{2}$$

$$N_{0j} = \frac{m_j}{2\mu_j} \tag{3}$$

In equation (2) ρ and σ_F denote the density and the strength, respectively, and γ is a semi-empirical statistical constant determining the dynamic fracture properties of the fragmenting shell material.

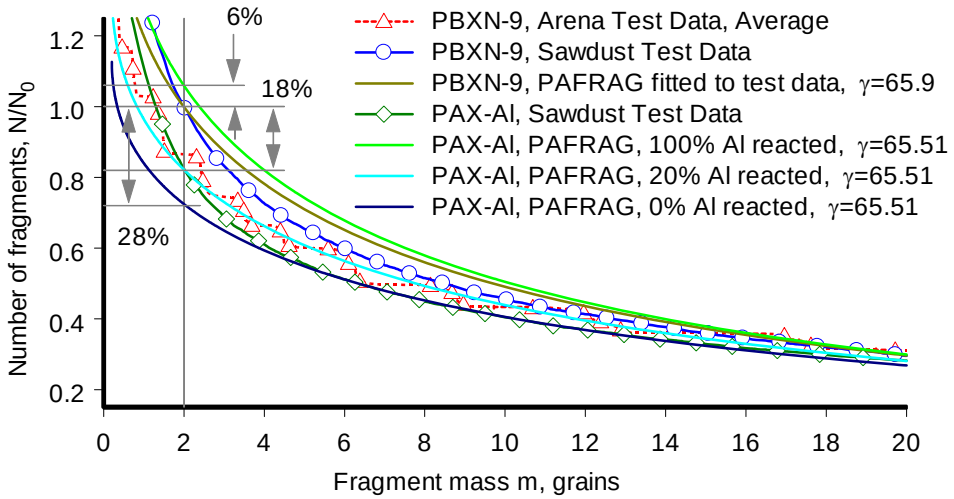

Fig. 2 Cumulative number of fragments versus fragment mass, Charge B.

Fig. 2 shows plots of the cumulative number of fragments versus the fragment mass *m* for the prototype "Charge B" warheads loaded with the PBXN-9 and with the PAX-Al explosives. In this work, two independent fragmentation data sets had been available for the baseline PBXN-9 warhead: (1) three full-scale fragmentation arena tests, and (2) one sawdust fragment recovery test. Referring to the figure, the "step-like" shape of the curve of data set (1) is common for all fragment mass distribution data compiled from "Z-data" or "JMEM" (Joint Munition Effectiveness Manual) data files[4]. The characteristic "steps" in the curve are because the original fragment mass distribution obtained from the fragmentation arena tests had been averaged and transformed into a distribution of a series of fragment "bins", or fragment weight classes. On the other hand, the sawdust recovery data files (2) obtained by weighting individual fragments represent the actual fragment number distribution, not that of the fragment weight classes. Accordingly, when comparing curves from the two sets, one should consider that the "original" curve of the data set (1) could be "passing" anywhere in the region covered by the height of the "steps".

Referring to the figure, the 10% to 20% discrepancy between the two PBXN-9 data sets is attributed to the disparity in the fragment mass recovery rates between the two techniques. For the fragmentation arena tests, the fragment recovery rates are typically in the order of 5% (of the total fragment mass), whereas for the sawdust experimentation, the recovery rates are usually better than 96% with less than 3% of shot-to-shot variations. Accordingly, the analytical PBXN-9 curve shown in the figure had been obtained through "fitting" the PAFRAG-Mott model with the data (2), and the data set (1) was used only for a baseline reference. All PAFRAG analyses presented in this work had been performed under an assumption that the fragmentation occurs instantly at approximately 3 volume expansions of detonation products. The curve "fitting" had been accomplished through varying the value of the fracture parameter γ in equation (2), aiming to achieve the best agreement between the analyses and the recovered cumulative number of fragments $N(m)$ for fragments with masses

greater than 2 grains, m=2. As shown in Fig. 2, the best agreement between the analyses and the data was for γ=65.9.

To examine parameters affecting the fragmentation performance of munitions with changes of the explosives, consider an analytical expression for the average fragment size, equation (2). Denoting explosive compositions PBXN-9 and PAX-Al by indices "1" and "2", and assuming that the fragment shape coefficient α, the flow stress at fracture σ_F, and the fracture radii r are approximately the same; the ratio of the total number of fragments is given by the equation

$$\frac{N_2}{N_1} = \left(\frac{\gamma_2}{\gamma_1}\right)^{3/2} \left(\frac{V_2}{V_1}\right)^3 \tag{4}$$

Since the PAFRAG-Mott distribution function, equation (1), is a monotonically increasing function of the fragment mass m, equation (4) represents the extremum of possible variances of the cumulative number of fragments. Equation (4) identifies two major parameters affecting the fragmentation performance of explosive fragmentation munitions: the fragment velocities V and the fracture parameter γ. The fragment velocities V are proportional to the amount of the thermochemical energy released by the detonating explosive when the later is fully or partially captured and transformed into the mechanical kinetic energy of the dilating metal shell; for the conventional high-brisance explosives the values of V are usually well defined empirical functions of the brisance and the density of explosive compositions. In the case of the "non-ideal" blast-enhanced aluminized explosives, the amount of the thermochemical energy released by the explosive is a strong function of the heat generated from the aluminum oxidation reactions using the oxygen supplied by the explosive and forming the alumina, Al_2O_3, albeit the exact the physical mechanism and extent of the contribution of this energy to the velocity of the dilating case is not fully clear.

Table 1: PAX-Al (18.1% Al) JWL EOS parameters from Stiel, ref. 5.

Parameter	**Mass fraction of Al reacted**				
	0%	**20%**	**25%**	**50%**	**100%**
A_1, *MBar*	17.3474	25.8870	24.8674	14.7220	20.2289
A_2, *MBar*	0.767133	0.836872	0.817133	0.534935	0.607504
R_1	6.40143	7.21178	7.17080	6.27772	7.13187
R_2	0.280505	2.14445	2.11846	1.79805	1.78257
ω	0.280505	0.283497	0.280392	0.258928	0.211775
ρ, g/cm^3	1.866	1.866	1.866	1.866	1.866
D_{CJ}, *m/sec*	8,049	7,973	7,956	7,846	7,664
P_{CJ}, *GPa*	29.316	29.102	29.193	29.482	29.197
E_0, *MJ/Kg*	4.396	4.982	5.060	5.776	7.306

The detonation parameters of both the PBXN-9 and the PAX-Al explosives that have been used in this work where adopted from thermochemical equilibrium analyses performed by Professor L. I. Stiel using the JAGUAR computer code[5]. The thermochemical models for both explosives had been correlated with the available one-inch copper cylinder test data, the detonation velocity data, and the detonation dent plate data. In the case of the PAX-Al explosive, the effect of the extent of the aluminum oxidation reaction had been modeled by "splitting" all the available aluminum into fixed "reactive" and "inert" fractions and allowing the "reactive" portion of the aluminum to compete for oxygen with other detonation decomposition species present. The resulting set of the PAX-Al JWL EOS (Jones-Wilkins-Lee Equation of State) parameters for varying the aluminum reaction fractions is given in Table 1. Comparing the JAGUAR analytical model predictions of cylinder wall velocities with the experimental data suggested no aluminum reaction for the one-inch copper cylinder test configuration[5].

According to the Mott's theory of fragmentation, the fragment velocities determine the rate at which stress relieved regions spread through the plastically expanding shell, which defines the average circumferential size and the mass of fragments. Thus, for an example, if the entire aluminum reacts before the fragmenting case breaks-up, the heat of the aluminum combustion can potentially significantly increase the fragment velocities, and the resulting fragmentation performance gain will be a strong function of the extent of the reaction and the rate. Conversely, if no appreciable fraction of aluminum reacts before the fragmenting case breaks up and the detonation products escape into the air, the aluminum powder additive is useless and the fragmentation performance of the warhead will be decreased. Accordingly, as given by equation (4), since the total number of fragments is proportional to the velocities in the power of three, the munition fragmentation performance should be very sensitive to the extent of the aluminum combustion.

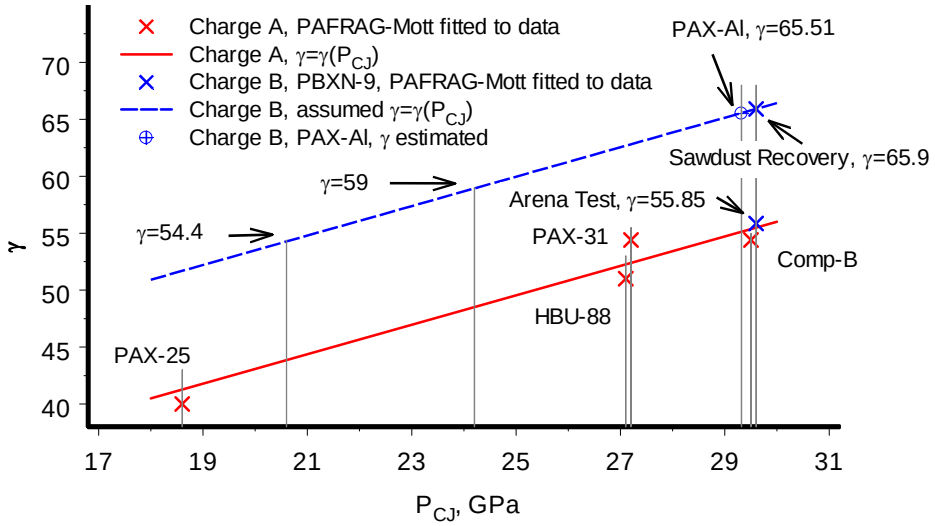

Fig. 3 Parameter γ versus explosive detonation Chapman-Jouguet (CJ) pressure

The second parameter that defines the fragmentation performance is the fracture parameter γ. For the PAX-Al prototype "Charge B" warhead, the value of the fracture parameter γ was established as follows. Fig. 3 shows a plot of the parameter γ versus explosive detonation Chapman-Jouguet (CJ) pressures, P_{CJ}. As shown in the plot, the values of γ for the prototype "Charge A" warhead[6] had been obtained through "fitting" the PAFRAG-Mott model analyses with the available experimental data of a series of explosive compositions with varying P_{CJ}, resulting in an approximately linear relationship between the fracture parameter γ and the P_{CJ}.

A detailed discussion of these analyses including the prototype "Charge A" warhead data can be found in reference [6]. As shown in Fig. 3, the $\gamma(P_{CJ})$ function for the prototype "Charge B" munition had been defined as a straight line parallel to that of the prototype "Charge A" warhead and passing through a "known" PBXN-9 γ-point, γ=65.9 at P_{CJ}=29.6*GPa*. The P_{CJ}=29.6*GPa* value used in this work had been estimated using the thermochemical analyses with the JAGUAR code[5] and is in a fair agreement with the 29.7 *GPa* to approximately 31.2 *GPa* values reported by Baudler et al[7]. As shown in Table 1, the JAGUAR-code estimates of the Chapman-Jouguet pressures for the aluminized PAX-Al composition are quite insensitive to the aluminum oxidation reaction extent; hence, the "0% aluminum reaction" P_{CJ} value of approximately 29.2 *GPa* had been used in this work. Accordingly, as shown in Fig. 3, for the PAX-Al prototype "Charge B" warhead, using P_{CJ}=29.2*GPa*, γ=65.51. Once the value of the fragmentation parameter γ for the PAX-Al prototype "Charge B" warhead had been established, all analytical PAFRAG PAX-Al curves shown in Fig. 2 were obtained using γ=65.51.

Refer back to Fig. 2. As shown in the figure, based on the sawdust fragment recovery data, PBXN-9 explosive produces approximately 18% more fragments with mass greater than 2 grains than that of the PAX-Al explosive. A quick analytical estimate of the relative fragmentation performance of the PBXN-9 and PAX-Al can be obtained using equation (4). From the available one-inch copper cylinder wall velocity data: V_1 =1.74*km/sec* for PBXN-9[7], from the average of six tests V_2 =1.63*km/sec* for PAX-Al[8]. Thus, V_2/V_1=0.94; using γ_1=65.9 and γ_2=65.51 equation (4) predicts N_2/N_1 of approximately 0.81, which is in excellent agreement with the sawdust experimental data. It should be noted that the quoted velocities had been measured at 19*mm* wall displacement, *i.e.*, a distance equivalent to approximately 6.8 detonation products volume expansions. Since, typically, the warhead steel cases fracture much earlier, at approximately 3 volume expansions; the wall-thickness-scaled copper cylinder test velocities represent the upper bound of velocities that can be achieved in fragmentation munitions, assuming that the extent of the explosive energy release is independent of the warhead caliber.

A series of solid PAX-Al curves shown in Fig. 2 represent PAFRAG predictions of the cumulative number of fragments versus fragment mass for the varying extent of the aluminum reacted. As shown in the figure, if no aluminum reacted, the cumulative number of the PAX-Al test fragments $N(m)$ for fragments with masses greater than 2 grains, m=2 had to be approximately 10% lower than that observed experimentally. On the other extreme, if 100% of the aluminum reacted, the number of fragments would be approximately 24% higher. Since the repeatability of the sawdust fragmentation recovery experimentation is usually very good (the deviation of the cumulative number of fragments is typically within approximately 3%), both the 0% and the 100% aluminum reaction chances would be highly unlikely. Accordingly, the extent of the aluminum reacted was determined by varying it until the best fit with the experimental data was achieved. As shown in Fig. 2, the best agreement between the analyses and the data was for the 20% aluminum reaction.

It should be noted that the above 20% aluminum reaction assessment is a function of the assumption of the fracture parameter value of γ=65.51 (estimated from the JAGUAR-code prediction of detonation pressures of approximately 29.2 *GPa*). The higher values of γ above 65.9 are unlikely; however, if a lower value of the fracture parameter γ is considered, the prediction of the extent of the aluminum oxidation reaction can be significantly higher. Unfortunately, to resolve the uncertainty in γ, no data on the direct measurement of the PAX-Al Chapman-Jouguet detonation pressures is available, except for the witness dent-plate data reported by Balas-Hummers[9], wherefrom the PAX-Al P_{CJ} is estimated at approximately 20%

lower value, at approximately 24.2 *GPa*. Accordingly, using P_{CJ}=24.2*GPa* with the $\gamma(P_{CJ})$ function of Fig. 3, γ=59. Consequently, to maintain the observed 18% difference between the PAX-Al and the PBXN-9 fragment number counts, equation (4) requires the PAX-Al over the PBXN-9 fragment velocity ratio to be in the order of V_2/V_1=0.99. Jumping ahead to the end of the paper and referring to Fig. 7, assuming a full 100% aluminum reaction the predicted PAX-Al to PBXN-9 velocity ratio is approximately 3% higher, V_2/V_1=1.03.

FRAGMENT VELOCITY MODELING AND EXPERIMENTATION

As discussed above, knowledge of reliable and consistent measurements of fragment velocities at the time when the warhead case breaks up is essential for a dependable assessment of performance of fragmentation munitions. In this work, fragment velocities of the prototype "Charge B" warhead had been assessed using a series of flash-panel measuring devices. The test summary with a detailed description of the flash-panel devises and the employed test arrangement is given by Grove[10]. The fragment velocity issues encountered and discussed in this work are mainly with the fidelity of the assessment of fragment velocities derived from the flash-panel velocity measuring devices.

Consider a fragment of mass *m* and presented area $\overline{A}$ moving through air of density ρ with a velocity *V*. Following the JMEM approach[4], the fragment presented area is defined as $\overline{A} = 0.25 \cdot A$, where *A* is the total surface area of the fragment. Denoting the air drag coefficient as c_d and neglecting the possibilities of the fragment trajectory changes due to initial angular momentum, lateral drift, and tumbling, the Newton's law requires that

$$c_d \rho \overline{A} V^2 = m \frac{dV}{dt} \tag{5}$$

For fragmentation munitions with conventional or enhanced-blast explosives, the initial fragment velocities are typically well above 1.2 *km/sec*, or approximately Mach 3.5. From the data given by Shaw[11], Calvert[12] and Dunn and Porter[13], for Mach numbers above 2 to 3 the fragment air drag coefficients are approximately constant and do not change with velocities. Accordingly, assuming that for fragment flight distances considered in this work, the decelerating fragment velocities do not drop below Mach 2, the fragment drag coefficient c_d can be assumed approximately constant, and equation (5) can be integrated to yield the following equation

$$\alpha = \frac{V_{TOA}}{V_0} = \frac{Sc_d \, \overline{A}/m}{e^{Sc_d \, \overline{A}/m} - 1} \tag{6}$$

In equation (6), *S* is the distance traveled by a fragment to a flash-panel, V_0 is the fragment initial velocity, V_{TOA} is the fragment time of arrival (TOA) velocity, and α is the fragment velocity retardation factor defined as the ratio of V_{TOA} over V_0. In the flash-panel velocity tests, for each fragment impacting and puncturing the panel, the coordinates and the time of the each of the "flashes" are recorded, thus, the individual fragment TOA velocities can be assessed as

$$V_{TOA} = \frac{S}{TOA} \tag{7}$$

As given by equation (6), the fragment velocity retardation factor α is a strong function of the ratio of the fragment presented area to the mass. Following the JMEM approach[4], assuming

approximately homologous shaped fragments, the fragment presented area to mass ratio is given by the following equation

$$\frac{\overline{A}}{m} = bm^{-1/3} = k^{-2/3}m^{-1/3} \tag{8}$$

In equation (8) coefficients *b* and *k* denote fragment shape factors; the coefficient *k* is in units of $[M][L]^{-3}$, the coefficient *b* is in units of $[L]^2[M]^{-2/3}$. Both above definitions are equivalent and acceptable; in this work, the shape factor *k* definition is used.

Figure 4 shows a series of plots of the fragment velocity retardation factor α, eq. (6), versus the flight distance *S* as functions of the fragment mass *m*, the fragment shape factor *k*, and the air drag c_d. The curves demonstrate possible ranges of systematic errors in α due innate uncertainties in the values of *m*, *k*, and c_d. For example, depending on the warhead caliber and the geometry, the fragment masses that hit TOA flash screens can vary as much as by two or three orders of magnitude: for the majority of fragmentation munitions, the fragment mass ranges from 0.5 to 50 *grains* are very common. Accordingly, an analytical estimate of the average fragment mass *m* and the ranges of possible fragment shape factors *k* should be of interest.

Refer to an idealized fragment shape shown in the left bottom corner of Fig. 4. Let the fragmenting shell thickness at the time of the fracture be *t*. Denoting the initial outside radius and the initial thickness of the shell as R_0 and t_0, respectively, and assuming that the shell material is incompressible and breaks up at strain levels corresponding to approximately 3 volume expansions of detonation products, the thickness of the shell at the time of fracture can be estimated from the mass continuity condition as

$$t^2 + 2\sqrt{3}t + t_0\left(2R_0 - t_0\right) = 0 \tag{9}$$

Assuming that the predominant mode of the fragment formation is through high-strain-rate adiabatic shearing and that the idealized fracture planes are directed at approximately 45˚ angles, the expected circumferential fragment size *a* must be approximately equal to the thickness of the shell *t* at the time of break up. Assume that the length *h* of the idealized prism-shaped fragments is approximately twice the width, $h=2a$. Using a representative circumferential fragment size of $a \approx 5mm$ and a typical density of steel of $7.8g/cm^3$, the masses of the parallelepiped, the trapezoidal prism, and the small wedge fragments shown in the figure will be approximately 30 *grains*, 22.5 *grains*, and 7.5 *grains*, respectively. Noting that from the sawdust fragment recovery experiments, the average fragment masses for the PBXN-9 and the PAX-Al "Charge B" prototype warheads were approximately 8.02 *grains* and 25.9 *grains*, respectively, the idealized "small wedge" and the "trapezoidal prism" fragment masses can be scaled to match the average fragment mass obtained from the tests. For example, for the PBXN-9 "Charge B" prototype warhead the 7.5-*grains* "small wedge" scales to approximately 2.0 grains (=[7.5÷30]·8.02), and the 22.5-*grains* "trapezoidal prism" to that of approximately 6.0 *grains* (=[22.5÷30]·8.02).

If the shape of the fragment is defined, the value of the fragment shape factor coefficient *k* can be calculated from equation (8) through the following relationship

$$k = \frac{m}{\overline{A}^{3/2}} \tag{10}$$

Equation (10) is useful for an analytic estimate of a reasonable range of variations of the fragment shape factors. For example, within the framework of the idealized fragment shape assumptions considered, equation (10) estimates an approximately 75% variance range of the

fragment shape factor values: for the ideal "parallelepiped" shaped fragments, k=791*grains/in*^{3}; for the "trapezoidal prism", k=1116*grains/in*^{3}; and for the "small wedge", k=640*grains/in*^{3}. For natural fragmentation munitions the fragments produced are usually rugged and irregular shaped, and the average values of k are functions of the shell material, the geometry, the thickness, the explosive, *etc*. The empirical values of the fragment shape factors are usually established by weighing the individual fragments with precision electronic scales and measuring their average projected areas using the icosahedron gage technique. The icosahedron gage is an electro-optical devise that throws a shadow of a fragment on an electronic sensing surface resulting in an automated digital readout of the projected area. For example, from the JMEM manual[4], for demolition and general purpose bombs fabricated from forged steel, k=590*grains/in*^{3}; for fragmentation and penetration bombs, also fabricated from forged steel, k=670*grains/in*^{3}; for warhead cases made of ductile iron, the values of the fragment shape factors k are approximately 50% higher, k=925*grains/in*^{3}. Based on the McCleskey data[14] of measurements of 94 fragment samples of four naturally fragmenting munitions of varying geometry, caliber, steel, and explosive fill composition, the fragment shape factors k can vary from approximately 400 *grains/in*^{3} to approximately 900 *grains/in*^{3}, that is, with approximately 125% variance for all fragment samples considered. However, for any individual munition considered, the variance of k was approximately 75%, which is in good agreement with an analytical estimate of this work.

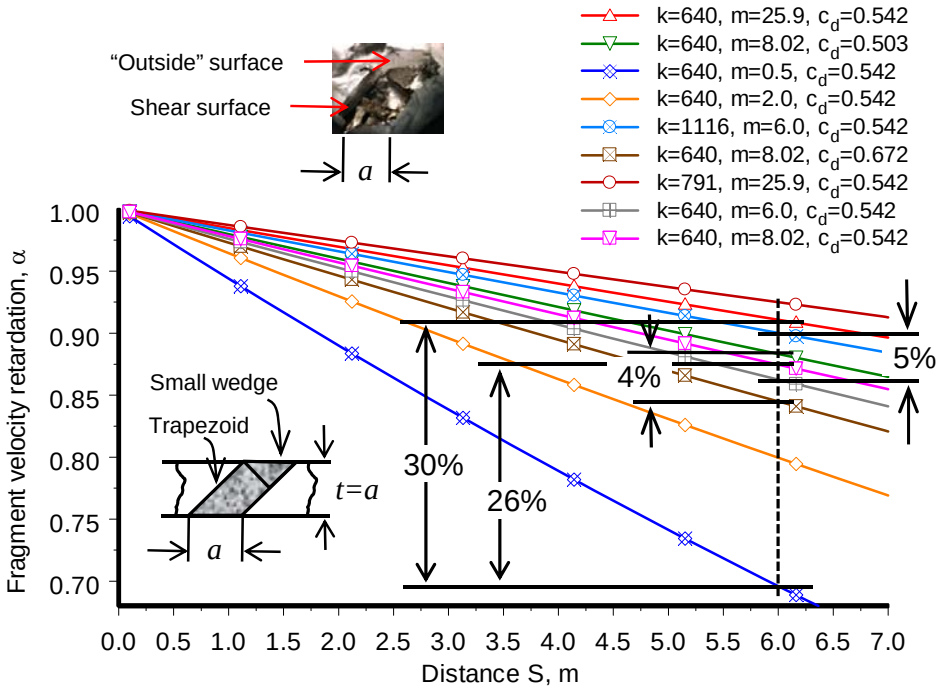

Fig. 4 Fragment velocity retardation factor α versus fragment flight distance *S*. Fragment shape factors k are *grains/in*^{3}, fragment masses m are in *grains*.

Let us first consider the error in the fragment velocity retardation factor $\Delta\alpha_m$ due to uncertainty in the values of the fragment mass m, say between the minimum fragment mass, m_{min}, and the average, m_0. Referring to Fig. 4, consider the TOA flash panels positioned at approximately 6 m away from the charge and assume representative values of the fragment shape factors k of 640 *grains/in*^{3} and that of the air drag coefficients, c_d=0.542. Consider that the minimum fragment mass m_{min} that can be registered by the flash panels at a 6 *meter* standoff is approximately 0.5 *grains*. Accordingly, as shown in Fig. 4, given that the average mass of the PAX-Al warhead fragments is approximately m_0=25.9 *grains*, the average

fragment velocity retardation factor error $\Delta\alpha_m$ due to the uncertainty in the fragment mass *m* that hits the screen, $\Delta\alpha_m=(\alpha_{m0}-\alpha_{min})\div\alpha_{min}=0.3$. The error $\Delta\alpha_m$ is a function of the fragmentation warhead average fragment size $2\mu_0$ and with decreases in the $2\mu_0$, the $\Delta\alpha_m$ decreases. For example, as shown in Fig. 4, for the PBXN-9 "Charge B" prototype warhead with $2\mu_0\approx 8.02$*grains*, $\Delta\alpha_m=0.26$.

Let us now consider the error in the fragment velocity retardation factor $\Delta\alpha_k$ due to uncertainty in the values of the fragment shape factor *k*, say between k_1 and k_2. As discussed above, the analytic assumption of approximately 75% uncertainty in the fragment factors values *k* is fair. As shown in Fig. 4, using analytic $k_1=640$*grains/in*^{3} and $k_2=1116$*grains/in*^{3}, $\Delta\alpha_k=(\alpha_{k2}-\alpha_{k1})\div\alpha_{k1}=0.05$.

An estimate of the uncertainties in the values of the air drag coefficient c_d available from the literature is as follows. From Shaw[11], from measuring the time of flight of controlled fragmentation shell fragments projected with velocities of approximately Mach 6, $c_d=0.57\pm0.07$. From Dunn and Porter[13], from measuring the time of flight of gun launched fragments with Mach velocities from 2.5 to 5: for steel cubes, $c_d=0.542\pm0.039$; for right circular cylinders, $c_d=0.542\pm0.05$; for samples of fragments recovered from exploded munitions, $c_d=0.66\pm0.018$. As shown in Fig. 4, considering the maximum variance between $c_{d1}=0.503$ and $c_{d2}=0.672$, $\Delta\alpha_{Cd}=(\alpha_{Cd2}-\alpha_{Cd1})\div\alpha_{Cd1}=0.04$.

The norm of the total error of the fragment velocity retardation factor α due to the combined uncertainties in the fragment mass *m*, the fragment shape factor *k*, and the air drag coefficient c_d, will be

$$\Delta\alpha=\sqrt{\Delta\alpha_m^2+\Delta\alpha_k^2+\Delta\alpha_{Cd}^2} \tag{11}$$

Accordingly, for the PBXN-9 warhead, $\Delta\alpha=0.27$, for the PAX-Al warhead, $\Delta\alpha=0.31$. The $\Delta\alpha$ estimate using equation (11) assumes only uncertainties in *m*, *k*, and c_d and does not include any TOA instrumentation errors, which should be in the order of at least additional 5%. A detailed analysis of uncertainties in assessing the initial fragment velocities from the TOA data is given in Wert *et al.*[15]. According to Wert *et al*, the overall uncertainties in the initial fragment velocities can approach 25% to 30%. This figure is in good agreement with results of this work.

Fig. 5 shows a series of plots of the experimental and analytical fragment velocities versus polar angles Θ for the PBXN-9 "Charge B" prototype warhead. The solid dot plot shown in the figure represents computational PAFRAG/CALE cell velocities of the warhead case material at approximately 3 volume expansions. This plot represents the distribution of the fragment spray velocities, assuming an instantaneous case fracture and ejection of individual "computational-cell-size" fragments. The arena test fragment velocities shown in the figure had been assessed applying equation (6) and using the fragment flash-screen time of arrival (TOA) data and the Θ-zone-averaged fragment weights from the fiberboard panels. The flash-panel data represents TOA of the "outer edge" of the fragment spray "cloud" projected by the explosion, and, as shown in the figure, the resulting arena test velocities are in very good agreement with the computational cell data for $25^\circ\le\Theta\le120^\circ$. The significant disagreement between the arena test data and analyses for Θ-zones with $\Theta<25^\circ$ and $\Theta>120^\circ$ is attributed to overestimating the velocities due the fragment mass, the shape factor, and the air drag coefficient assumptions.

The plot of the flash-screen TOA velocity averages shown in Fig. 5 represents the arithmetic average of the individual TOA velocities:

$$V_{TOAj} = \frac{\sum_{l}^{L_j} \frac{S_l}{TOA_l}}{L_j} \tag{12}$$

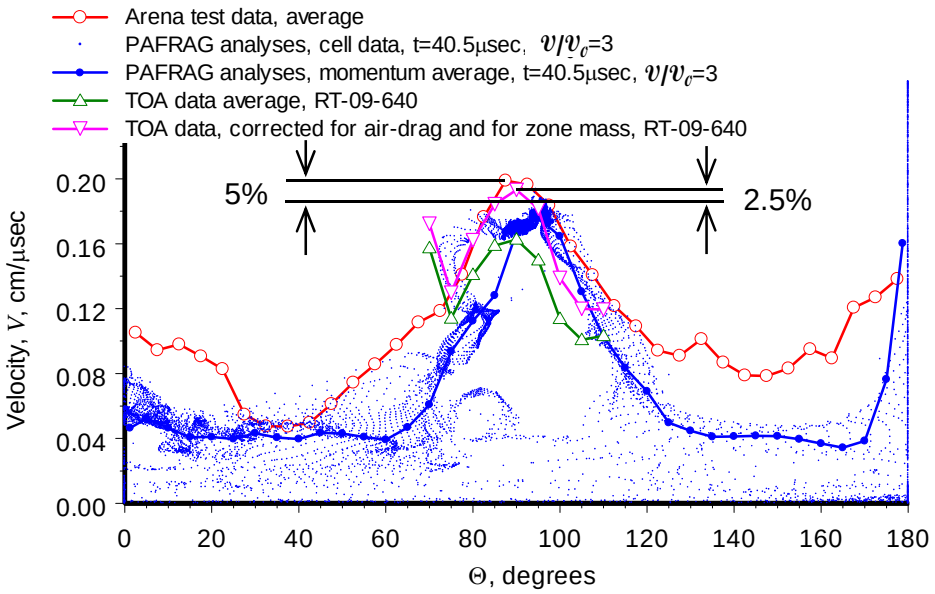

Fig. 5 Fragment velocities versus polar angle Θ. Charge B, PBXN-9 explosive.

In equation (12) S_l is the distance traveled by a fragment l to the flash-panel, TOA_l denotes the time of arrival of fragment l, and L_j is total number of the flash-panel fragment "hits" in any given Θ_j-zone. The flash-screen TOA velocities corrected for the air-drag and the fragment mass shown in Fig. 5 had been assessed as follows:

$$V_{0j} = \frac{\sum_{l}^{L_j} \frac{S_l}{TOA_l \cdot \alpha_{lj}}}{L_j} \tag{13}$$

In equation (13) α_{lj} denotes the velocity retardation of a fragment l in the j-th Θ-zone. Applying equations (6) and (8), the individual fragment retardation factors α_{lj} are as follows:

$$\alpha_{lj} = \frac{S_l c_d k^{-2/3} m_{0j}^{-1/3}}{e^{S_l c_d k^{-2/3} m_{0j}^{-1/3}} - 1} \tag{14}$$

The flash-panel TOA velocities corrected for the air-drag and the fragment mass shown in Fig. 5 had been calculated using representative values of the air drag coefficient, c_d=0.542, and the fragment shape factor, k=640*grains/in*^{3}, both parameters constant for all Θ-zones considered. The average fragment mass m_{0j} of fragments expected to hit the *j-th* Θ-zone had been calculated using the following scaling relationship:

$$m_{oj} = \frac{\mu_j}{\mu_0} m_{0\exp} \tag{15}$$

In equation (15) $m_{0\exp}$ denotes the total average fragment mass obtained from the sawdust experimentation ($m_{0\exp}$=8.02*grains* for the PBXN-9 "Charge B" prototype warhead), μ_j and μ_0

are the average one-half fragment masses for the *j*-th Θ-zone and the total, respectively, both determined from the PAFRAG analyses.

As shown in Fig. 5, for the Θ-zones in the range of 75˚≤Θ≤95˚, the flash-screen velocities are in very good agreement with both the arena test data and the computational cell data. It is interesting to note, that the sharp "surge" of fragment velocities for the approximately 70˚ degree Θ-zone range is in a very good agreement with the computational cell data predictions. However, this fragment velocity "surge" is absent in the arena test data, possibly, because of "smoothing" assumptions applied in the experimental data filtering. The disagreement between the flash-screen velocity data and that of both the arena test data and the PAFRAG analyses for the 95˚≤Θ≤110˚ range should also be noted, in particular, that of the slope and of the Θ-axis "shift". The disparity is attributed to the instantaneous case fracture assumptions resulting in PAFRAG inaccuracies in assessing m_{0j} values for these zones.

Fig. 6 shows a series of plots of the experimental and analytical fragment velocities versus polar angles Θ for the PAX-Al "Charge B" prototype warhead. As shown in the figure, two analytical possibilities had been considered: the 20% aluminum reaction extent case and that if the entire 100% of aluminum is reacted; the two assumptions resulting in approximately 6% difference in the main-spay fragment velocity predictions. The PAX-Al flash-panel fragment velocities shown in the figure had been calculated from the time of arrival data under the same set of assumptions as that of the PBXN-9 "Charge B" prototype warhead: the air drag coefficient, c_d=0.542, and the fragment shape factor, k=640*grains/in*^{3}, both constant for all Θ-zones considered. Also, similar to the PBXN-9, the PAX-Al Θ_j-zone-variable average fragment mass m_{0j} parameter had been calculated applying equation (15) employing m_{0exp}=25.9*grains* from the sawdust recovery experiments. Both the 20% aluminum reacted and the 100% aluminum reacted assumptions had been considered, resulting in negligible differences in the flash-screen velocity estimates (see Fig. 7).

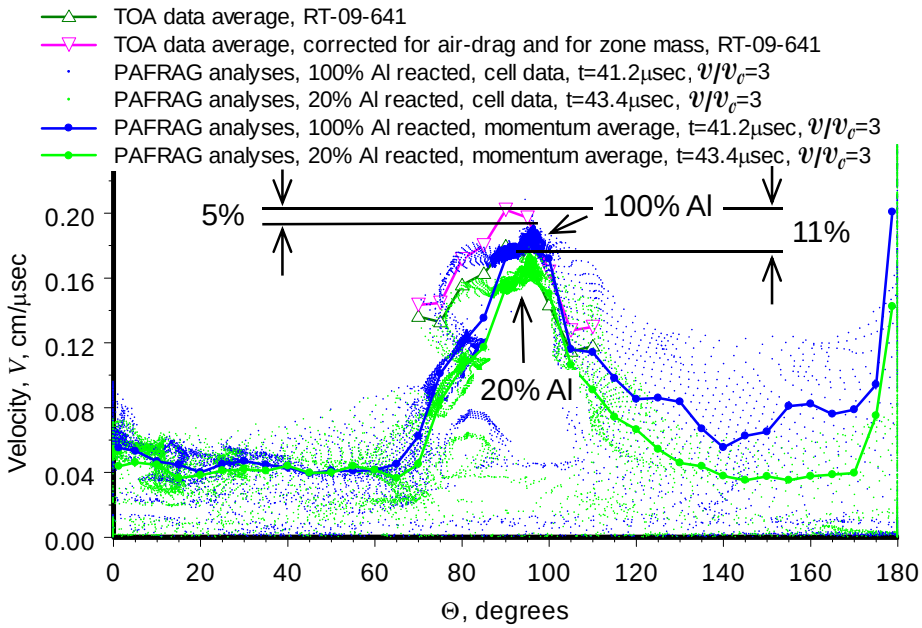

Fig. 6 Fragment velocities versus polar angle Θ. Charge B, PAX-Al explosive.

As shown in Fig. 6, the 100% aluminum reaction assumption seems to better agree with the flash-screen test velocities than that of the 20%, for both, the main fragment spay range, and the 70˚≤Θ≤95˚ range. It also should be noted, that for the 95˚<Θ≤110˚ range, all analyses significantly disagreed with the flash-panel test data, both, in the slope, and in the Θ-axis

"shift". Similar to the PBXN-9 "Charge B" prototype warhead, the disparity is attributed to the instantaneous case fracture assumptions leading to inaccuracies in the m_{0j} values. In addition, the rate of the explosive energy release modeling may be another face of the issue.

As discussed above, the uncertainty of the flash-panel velocity data is within approximately 30% error margin. Yet, as shown in Fig. 6, in the main fragment spray range, the deviation of the flash-panel data from the fragment velocity predictions is approximately 5% for the 100% aluminum reaction assumption, and that of approximately 11%, for the 20% aluminum reaction assumption. Accordingly, based on the flash-panel data collected, the extent aluminum reaction in the PAX-Al "Charge B" prototype warhead cannot be established with any acceptable level of confidence.

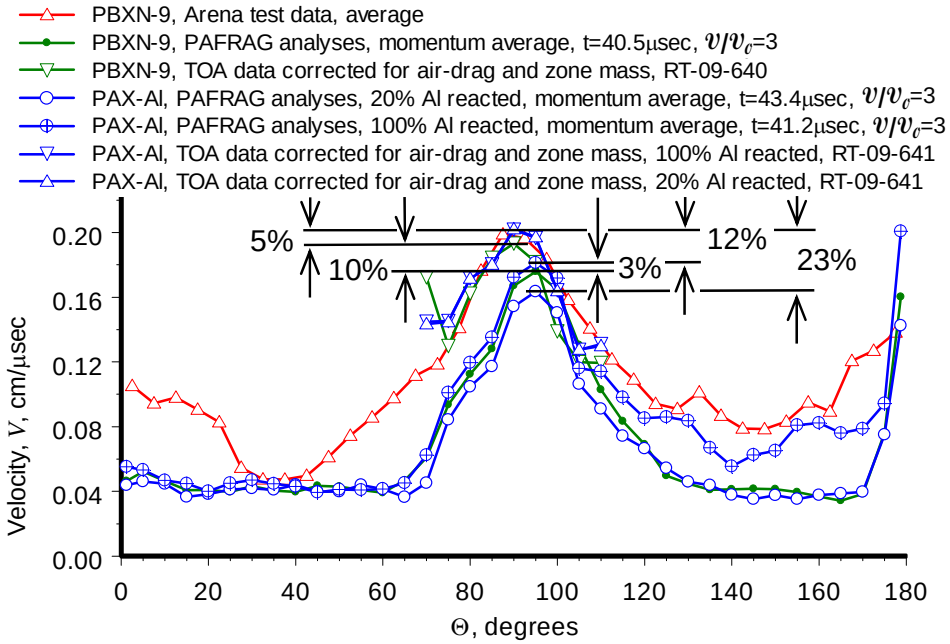

Fig. 7 PBXN-9 and PAX-Al fragment velocities versus polar angle Θ. Charge B.

Fig. 7 shows a series of plots of the experimental and analytical fragment velocities versus polar angles Θ for the PBXN-9 and the PAX-Al "Charge B" prototype warheads. The series of plots marked by circles correspond to analytical curves of the momentum average fragment velocities from the PAFRAG analyses. Momentum averaged fragment velocities represent the extent of the thermochemical energy released by the explosive that had been captured into the fragment kinetic energy before the warhead case fractures and the products of detonation escape into the surrounding air. As shown in the figure, the increase in the aluminum reaction extent from the 20% to that of 100%, increases fragment velocities by approximately 11%. This corresponds to approximately 23% in the increase of the kinetic energy transmitted to the fragments, while, from the data of Table 1, the relative increase in the available thermochemical energy is 47%, indicating approximately 50% losses into heat.

Unfortunately, the momentum average fragment velocities cannot be directly compared with the fragmentation arena or the flash-screen test velocities, only the relative numbers thereof. For example, Fig. 7 shows approximately 10% variance between the momentum average velocities and the flash-screen test data for PBXN-9, approximately 12% for the 100% aluminum reacted PAX-Al, and approximately 23% for the 20% aluminum reacted PAX-Al. These numbers are in a good agreement with the approximately 5% variance between the computational cell data and the flash-panel velocities for PBXN-9 of Fig. 5, that of 5% for the

100% aluminum reacted PAX-Al, and that of 11% for the 20% aluminum reacted PAX-Al, both of Fig. 6.

The series of curves marked by triangles represent plots of the experimental data from the PBXN-9 arena fragmentation tests and from the flash-screen velocity tests, both for the PBXN-9 and the PAX-Al explosives. As shown in the Fig. 7, the approximately 5% difference between the flash-screen velocities of PAX-Al and PBXN-9 is in a good agreement with the approximately 3% difference between the PAFRAG calculated momentum average velocities of the 100% aluminum reacted PAX-Al assumption and that of the PBXN-9. It is interesting to examine the implication of this number using the fragment recovery test data. As discussed in the preceding section, assuming PAX-Al Chapman-Jouguet detonation pressure of P_{CJ}=24.2 *GPa*[9] and employing the observed 18% difference between the PAX-Al and the PBXN-9 fragment number counts, equation (4) requires that the PAX-Al over the PBXN-9 fragment velocity ratio be in the order of approximately V_2/V_1=0.99. Similarly, assuming the momentum average velocity ratio of V_2/V_1=1.03 and employing the observed 18% difference between the PAX-Al and the PBXN-9 fragment number counts, applying equation (4) and the $\gamma(P_{CJ})$ function of Fig. 3 results approximately in γ=52.4 and P_{CJ}=20.6 *GPa*. The later is a relatively low number, for example, for reference: for TNT, P_{CJ} is approximately 21 *GPa*.

CONCLUSIONS

A new modeling and experimentation methodology for assessing fragmentation characteristics of blast-enhanced explosive fragmentation munitions has been developed. Fragmentation performance of two high explosive compositions has been examined in this work: a baseline, PBXN-9 (92% HMX, 6% Dioctyl adipate, 2% Hycar 4454) explosive, and an aluminized blast-enhanced PAX-Al. The experimental assessment of the fragmentation performance of tested charges was accomplished using the fragmentation arena tests, the sawdust fragment recovery experimentation, and the flash-screen fragment velocity tests. The analytical assessment of the thermodynamic parameters of the PBXN-9 and the PAX-Al compositions was performed employing the JAGUAR code. The analytical assessment of the fragmentation parameters of the explosive fragmentation charges was performed employing the PAFRAG (Picatinny Arsenal Fragmentation) modeling methodology linking the three-dimensional axial symmetric high-strain high-strain-rate hydrocode analyses with a phenomenological fragmentation model based on the Mott's theory of break-up of ideal cylindrical "ring-bombs". For the PBXN-9 explosive, the PAFRAG modeling has been shown to accurately reproduce the available experimental data, both the fragmentation and the fragment velocity measurements. However, for the PAX-Al explosive, a significant discrepancy between the one-inch copper cylinder velocity test, the fragment recovery data, and the flash-screen velocity data had been noted and examined. Comparing the JAGUAR analytical model predictions with the PAX-Al experimental data suggests no aluminum reaction for the one-inch copper cylinder test configuration is occurred. However, based on the fragment recovery data, the coupled PAFRAG/thermodynamic analyses indicated that the amount of the aluminum contributing to the momentum of the fragments had to be in the order of approximately 20% of the total available, 80% of the aluminum remaining unreacted. Conversely, from the flash-screen velocity data, the entire 100% aluminum available had to react to agree with the relatively fast fragment time of arrivals measured. The data confidence level of the flash-screen velocity technique was examined, indicating approximately 30% data uncertainty margins possible. Accordingly, the entire 100% aluminum reaction may or may not be feasible, but a fair chance of approximately 20% of the aluminum contributing to the

fragment kinetic energies had been concluded. To resolve the issue a series of additional two-inch and four-inch PAX-Al cylinder detonation velocity tests have been suggested and are underway.

ACKNOWLEDGEMENTS

Special thanks to Dr. B. D. Fishburn of Science Applications International Corporation, Picatinny Arsenal, New Jersey, for many valuable discussions and insights. Messrs. J. R. Kraft and J. Pham of US Army Armament Research Development and Engineering Center are acknowledged for arranging and coordinating the sawdust and flash-panel velocity experiments. Messrs. D. Sato, W. Grove, and D. Boeka of General Dynamics Corporation, Ordnance and Tactical Systems, Niceville, Florida, are acknowledged for directing sawdust and flash-panel velocity experiments and providing the experimental data. Ms. W. A. Balas Hummers of US Army ARDEC is acknowledged for providing data on the PAX-Al explosive. Professor L. I. Stiel of Polytechnic Institute of New York University is acknowledged for his contributions in thermochemical equilibrium modeling. Mr. E. Jelis of US Army Armament Research Development and Engineering Center is acknowledged for providing high resolution images and metallurgical analysis of fragments. Messrs. L. Sotsky and A. J. Mock of US Army Armament Research Development and Engineering Center are acknowledged for providing initiative, support and funds that made this work possible.

REFERENCES

[1] V. M. Gold, 2007, An Engineering Model for Design of Explosive Fragmentation Munitions, Technical Report ARAET-TR-07001, Picatinny Arsenal, New Jersey.

[2] R. E. Tipton, 1991, CALE Users Manual, Version 910201, Lawrence Livermore National Laboratory, Livermore, California.

[3] V. M. Gold, E. L. Baker, W. J. Poulos, and B. E. Fuchs, 2006, PAFRAG Modeling of Performance of Explosive Fragmentation Munitions, Int. J. Imp. Engng., Vol. 33, pp. 294-304.

[4] Joint Munition Effectiveness Manual, 2009, Test and data reduction procedures for munitions, Report FM 101-51-3, Revision 4, Joint Technical Coordination Group for Munition Effectiveness, Aberdeen Proving Ground, Maryland.

[5] L. I. Stiel, 2008-2010, JAGUAR PAX-Al JWL EOS, unpublished work, Polytechnic Institute of New York University, Six MetroTech Center, Brooklyn, New York.

[6] V. M. Gold, 2009, Modeling performance of blast-enhanced explosive fragmentation munitions, Int. Workshop on Structures Response to Impact and Blast, Haifa, Israel.

[7] B. Baudler, R. Hutcheson, M. Gallant, and J. Leahy, 1989, Characterization of the PBXW-9, Technical Report NSWC TR 86-334, Naval Surface Warfare Center, Dahlgren, Virginia.

[8] B. Fuchs, 2008, PAX-Al copper cylinder tests, unpublished data, Picatinny Arsenal, New Jersey.

[9] W. Balas-Hummers, 2007, PAX-Al MR qualification, Briefing, Picatinny Arsenal, New Jersey.

[10] W. Grove, 2010, Fragmentation test data reduction and analyses for three HCEPW warheads, General Dynamics Corporation, Ordnance and Tactical Systems, Niceville, Florida.

[11] J. E. Shaw, 1950, A measurement of the drag coefficient of high velocity fragments, BRL Report No. 744, Ballistic Research Laboratories, Aberdeen Proving Ground, Maryland.

[12] J. A. Calvert, 1956, Ballistic tables for fragments, NPG Report No. 1494, U. S. Naval Proving Ground, Dahlgren, Virginia.

[13] D. J. Dunn, Jr. and W. R. Porter, 1955, Air drag measurements of fragments, BRL Memorandum Report No. 915, Ballistic Research Laboratories, Aberdeen Proving Ground, Maryland.

[14] F. McClesky, 1988, Drag coefficients for irregular fragments, Technical Report NSWC TR-87-89, Naval Surface Warfare Center, Dahlgren, Virginia.

[15] S. D. Wert, J. E. Prendergast, D. A. Landa, and J. F. Schneider, Improvements in munition fragment arrival time data acquisition, reduction, and analysis, Technical Report AFWL-TR-88-77, Air Force Weapons Laboratory, Kirtland Air Force Base, New Mexico.